coatings

Article

Preparation of Mortar with Fe_2O_3 Nanoparticles for Radiation Shielding Application

M. I. Sayyed [1,*], Nouf Almousa [2] and Mohamed Elsafi [3,*]

[1] Department of Physics, Faculty of Science, Isra University, Amman 66110, Jordan
[2] Department of Physics, College of Science, Princess Nourah Bint Abdulrahman University, P.O. Box 84428, Riyadh 11671, Saudi Arabia
[3] Physics Department, Faculty of Science, Alexandria University, Alexandria 21511, Egypt
* Correspondence: dr.mabualssayed@gmail.com (M.I.S.); m.elsafi.phy@alexu.edu.eg (M.E.)

Abstract: The current study aims to investigate the radiation shielding properties of mortar samples with Fe_2O_3 nanoparticles for radiation protection applications. For the reference mortar (free Fe_2O_3 nanoparticles) and the mortar with different concentrations of Fe_2O_3 nanoparticles, we experimentally measured the transmission factor (I/I0) for four different thicknesses of the prepared mortar. The I/I_0 results indicated that the transmission of the photons through the mortars decreases with increases in the mortar's thickness. The lowest TF was found for the mortar coded as MI-25 (contains 25 wt.% of Fe_2O_3 nanoparticles), which gives an indication about the development in the attenuation ability of the prepared mortar samples due to the addition of Fe_2O_3. Similarly, the linear attenuation coefficient (LAC) results showed an increasing trend with the addition of Fe_2O_3 nanoparticles for the four tested energies. These results confirm that increasing the ratio of Fe_2O_3 nanoparticles can lead to a remarkable improvement in the gamma ray shielding. We reported the half value layer (HVL) and we found that the HVL for the reference mortar at 0.06 MeV is 1.223 cm, while it changed from 1.19 to 1.074 cm for the mortar with 5 and 25 wt.% of Fe_2O_3 nanoparticles. The HVL results demonstrated that increasing the ratio of Fe_2O_3 nanoparticles can lead to a notable reduction in the HVL. The tenth value layer results proved that we can develop new mortars for radiation shielding applications by introducing more concentrations of Fe_2O_3 nanoparticles.

Keywords: Fe_2O_3 nanoparticles; mortar; transmission factor; half value layer

check for updates

Citation: Sayyed, M.I.; Almousa, N.; Elsafi, M. Preparation of Mortar with Fe_2O_3 Nanoparticles for Radiation Shielding Application. *Coatings* **2022**, *12*, 1329. https://doi.org/10.3390/coatings12091329

Academic Editor: Kuthati Yaswanth

Received: 19 August 2022
Accepted: 9 September 2022
Published: 12 September 2022

1. Introduction

Radiation offers many benefits when used in applications in the medical industry, energy generation, food processing, agriculture, and more. Radiation can save lives by eliminating tumors in radiotherapy and imaging using X-rays. However, despite these advantages, ionizing radiation can be very harmful to humans if they are exposed to these high-energy photons for long periods of time, as the radiation can rip electrons from atoms and cause permanent side effects [1–3]. Due to the naturally harmful nature of radiation, several methods are used in an attempt to reduce these effects. These include distancing oneself from the radiation source, minimizing the time exposed to radiation, and using radiation shields [4–6].

Radiation shields are materials that are placed between the radiation source and the human body and are specifically designed to absorb as many photons as possible for that specific application. Ideal radiation shields should be light, effective at absorbing a wide range of photons, thin, low cost, easy to manufacture, and have other factors. They vary from simple lead aprons to glasses, composites, polymers, alloys, and more. These materials are often enhanced using different micro- and nanoparticles, which are suited for the desired application [7–12].

One example of a radiation shielding material that is commonly used is concrete [13,14]. Nikbin, I. et al. [15] prepared heavy-weight concrete with varying amounts of nano bismuth oxide. Heavy-weight concrete aims to reduce the thickness of the shield by increasing the density of concrete through the use of heavy-weight aggregates. The mechanical and gamma ray shielding properties of the concretes improved when more bismuth oxide nanoparticles were added to the composition. Nikbin, I. et al. [16] studied the gamma ray shielding properties of introducing nanoparticle titanium oxide to heavy-weight concrete, finding a positive correlation between TiO_2 content and the attenuation abilities of the concretes. El-Sayed, T. [17] furthered previous research on heavy-weight concrete by analyzing the effect of adding rice straw ash on the shielding properties of the concretes, in an attempt to make use of a waste material. The study demonstrated that the sample with 3% polyethylene is the optimum concrete mix for shielding applications. El-Sayed, A. et al. [18] developed an artificial neural network to calculate radiation shielding parameters of concrete with different nanoparticle additives and then compared the predicted values with experimental results, finding a great agreement between the two methods, and proving the viability of the model.

Other materials, such as cements with different nanoparticles, are also being investigated for their radiation shielding potential. Abo-El-Enein, S. et al. [19] used hematite (Fe_2O_3) and ZnO nanoparticles to try to enhance the mechanical, thermal, and radiation shielding ability of ordinary Portland cement pastes. Additionally, mortar and concrete are being researched as a more environmentally friendly and cheaper alternative to ordinary Portland cement. Mortar by itself exhibits poor strength at ambient temperatures, but these properties can be greatly improved by adding different types of nanoparticles into the mix, as demonstrated by Seifan, M. et al. [20] when they introduced nanosilica and microsilica to fly ash mortar. Furthermore, Glinicki, M. et al. [21] evaluated the neutron shielding ability of mortar containing boron aggregates, discovering a positive linear relationship between the boron content of the samples and their shielding ability.

The current study aims to investigate the radiation shielding properties of mortar samples with Fe_2O_3 nanoparticles for various applications.

2. Materials and Methods

The mortar was prepared in the traditional way, and the same properties of cement and sand were published previously [22], where the cement was mixed with sand and then water was added, where the ratio of cement to water was 2:1, and stirred well to obtain a homogeneous mortar to obtain the control sample (MI-0), and then the Fe_2O_3 nanoparticles were added in proportions of 5, 10, 15, 20, and 25% of the amount of cement added to obtain the rest of the mortar samples as shown in Table 1. The samples were cut to fit the experimental measurement as shown in Figure 1. Fe_2O_3 nanoparticles were purchased from Nano-Tech Company in Egypt and their size was confirmed by photographing them using a transmission electron microscope (TEM). It was found that Fe_2O_3 nanoparticles are needles and rods with an average size of 100 ± 50 (length) and 15 ± 5 (width) nm as shown in Figure 2. The density was measured traditionally by the law of mass over volume, where samples are homogeneous in shape, the sample is weighed, and the volume is measured theoretically for a cylindrical sample [23].

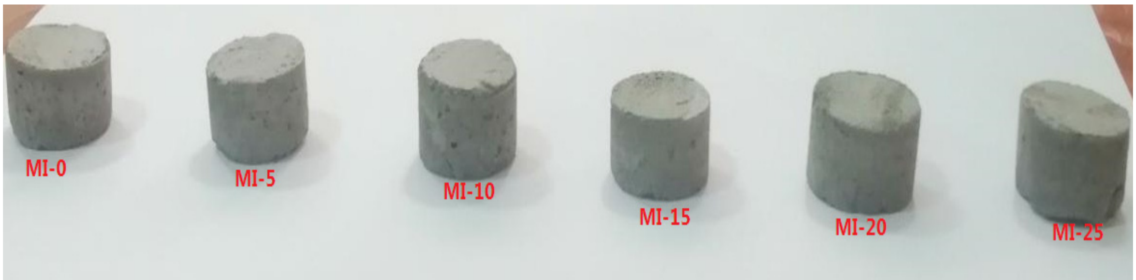

Figure 1. The mortar samples used in the radiation attenuation measurements.

Table 1. The composition of the prepared mortar (Kg/m^3).

Codes	Composition, Kg/m^3				Density, g/cm^{-3}
	Cement	**Water**	**Sand**	**Fe_2O_3 Nanoparticles**	
MI-0	500	250	1375	—	2.241
MI-5	500	250	1375	25	2.256
MI-10	500	250	1375	50	2.270
MI-15	500	250	1375	75	2.285
MI-20	500	250	1375	100	2.300
MI-25	500	250	1375	125	2.314

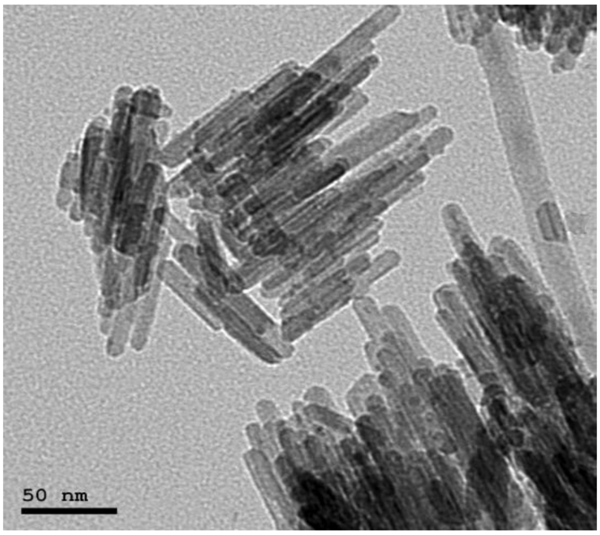

Figure 2. TEM micrograph for as-prepared hematite NPs.

The attenuation coefficient was measured experimentally only for the use of nanoparticles in the samples, but for the accuracy of the measurement by which the samples were measured, the control sample was compared with the XCOM program, and a very good agreement between the theoretical and experimental results was obtained. Three radioactive sources (Cs-137, Co-60, and Am-241) and an HPGe detector were used. The samples were placed as in Figure 3, and the counting rate was calculated using a program connected to the device (Genie 2000 program), where a sample of thickness t and counting rate N was calculated, then the sample was removed and the free counting rate was calculated (N_0) as shown in Figure 4 for the Cs-137 point source. From the count rate calculation, the linear attenuation coefficient (LAC) was calculated from the following formula [24–27].

$$\mathrm{LAC} = \frac{-1}{t} \ln \frac{N}{N_0} \quad (1)$$

The other shielding parameters were calculated based on previous works [28–33], such as HVL, MFP, TF, TVL, and radiation absorption ration (RAR) by the following equations.

$$\mathrm{HVL} = \frac{\ln(2)}{\mathrm{LAC}} \quad (2)$$

$$\mathrm{MFP} = \frac{1}{\mathrm{LAC}} \quad (3)$$

$$\mathrm{TVL} = \frac{\ln(10)}{\mathrm{LAC}} \quad (4)$$

$$\mathrm{TF} = \frac{\mathrm{I}}{\mathrm{I_0}} = \frac{\mathrm{N}}{\mathrm{N_0}} \tag{5}$$

$$\mathrm{RAR}\ (\%) = [1 - \mathrm{TF}] \times 100 \tag{6}$$

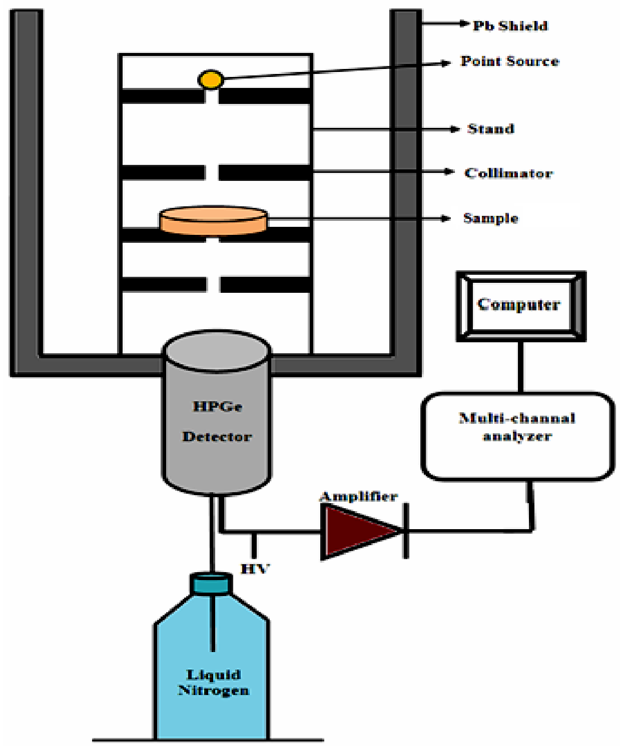

Figure 3. The arrangement of the experimental work.

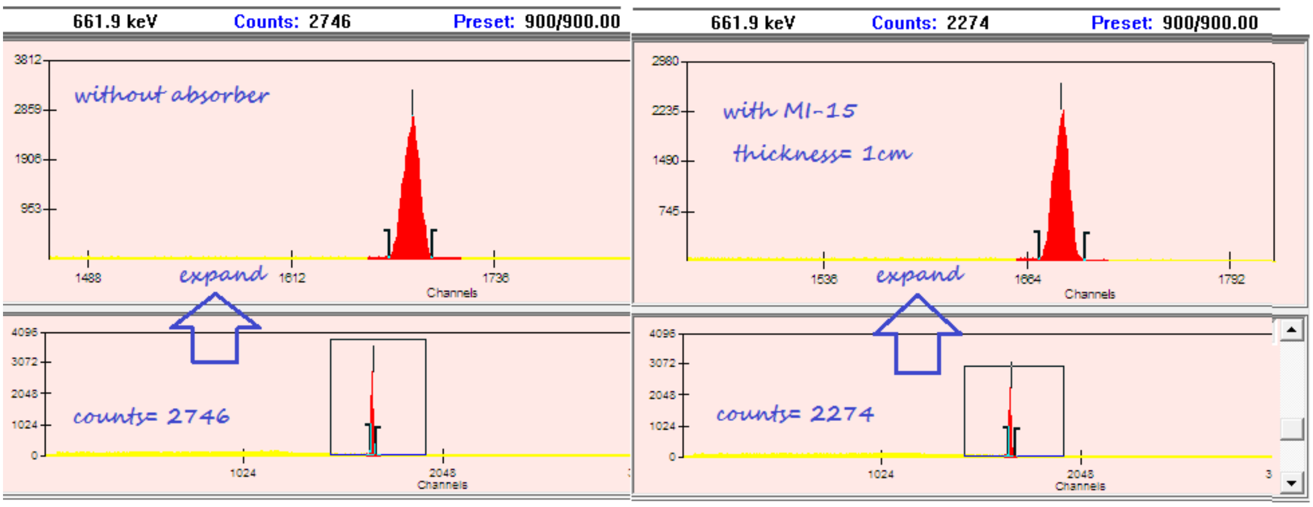

Figure 4. The spectrum with and without absorber at 0.662 MeV line.

3. Results and Discussion

The effect of the addition of nanosized Fe_2O_3 particles on the radiation attenuation performance of the prepared mortars was examined by using experimental results (see Section 2). Additionally, the radiation shielding abilities of the prepared mortars with nanosized Fe_2O_3 were compared to each other and we reported the influence of different thicknesses on the transmission of the photons through each sample. For the reference mortar (free Fe_2O_3 nanoparticles) and the mortar with different concentrations of Fe_2O_3 nanoparticles, we experimentally measured the transmission factor (I/I_0) for each thickness of the prepared mortar. We plotted I/I_0 versus the thickness of the mortar samples at the tested energies (Figure 5a–d). These are very useful figures, since from these figures we can understand the influence of the thickness on the transmission factor. In addition, from this figure, we can estimate the LAC for the reference mortar and the mortar samples with Fe_2O_3 particles. In each figure, we included the straight line fit equation, and we can notice that the slope of each equation is negative, which indicates that the parameter on the *Y*-axis (which is the TF) decreases with increases in the mortars' thickness. For the reference mortar, the straight line best fit equation at 0.060 MeV is y = −0.2868x + 0.8759. The absolute value of the slope represents the LAC at this energy (i.e., 0.06 MeV) which is equal to 0.5670 cm^{-1}. We can derive the MAC from the LAC. By dividing the LAC for each mortar by its individual density, we can derive the MAC at a given energy. All these critical parameters (i.e., TF, LAC, and MAC) have been determined for the reference mortar and mortar samples with Fe_2O_3 nanoparticles as we will discuss in the next paragraphs. It can be observed in Figure 5a–d that an increase in the thickness of the mortars led to a decrease in the TF and hence a decrease in the transmission of the photons through the prepared mortars under all the applied energies. Additionally, the lowest TF belongs to mortar coded as MI-25, which gives an indication about the development in the attenuation ability of the prepared mortar samples due to the addition of Fe_2O_3. In order to check the enhancement in the attenuation ability of these mortar samples due to the increase in the thickness and Fe_2O_3 contents, we will discuss the MAC and LAC, and other related parameters.

In Figure 6, we represented the LAC for the reference mortar and the samples with Fe_2O_3 nanoparticles as a function of Fe_2O_3. The LAC results display an increasing trend with the addition of Fe_2O_3 nanoparticles for the four tested energies. The lowest LAC has been reported for the reference mortar (free Fe_2O_3 nanoparticles) because it is composed of low atomic number elements. In contrast, the highest LAC is found for MI-25, which contains the maximum amount of Fe_2O_3. These results confirm that increasing the ratio of Fe_2O_3 nanoparticles can lead to a remarkable improvement in the gamma ray shielding. In addition to the impact of Fe_2O_3 nanoparticles on the LAC, we can see that the energy of the photons is another factor that changes the LAC values. When examining the LAC for a specific composition at 0.06 and 1.333 MeV, we can see a big difference in the LAC values between these two energies. The LAC for MI-10 (for example) at 0.06 MeV is 0.598 cm^{-1}, while it is only 0.1301 cm^{-1} at 1.333 MeV. The LAC values at low and high energies for the reference mortar and other mortar samples with Fe_2O_3 nanoparticles have the same trend as the LAC reported in other studies and for different materials [34–36].

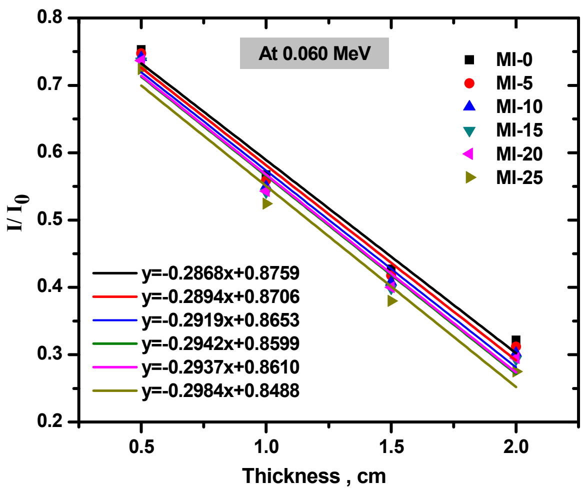

(a)

Figure 5. *Cont.*

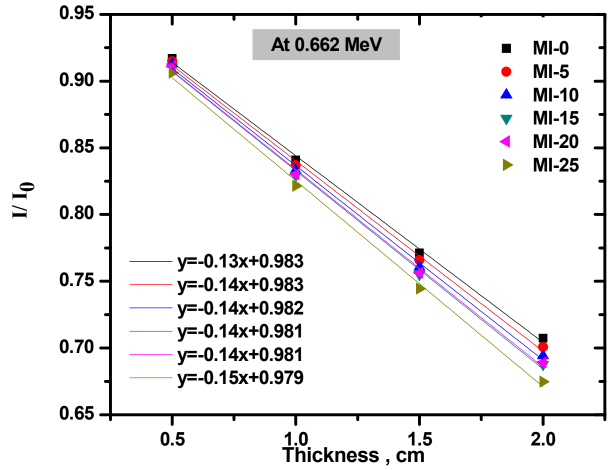

(**b**)

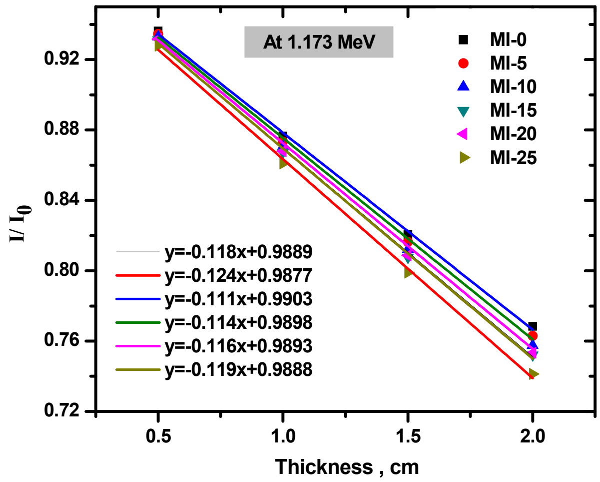

(**c**)

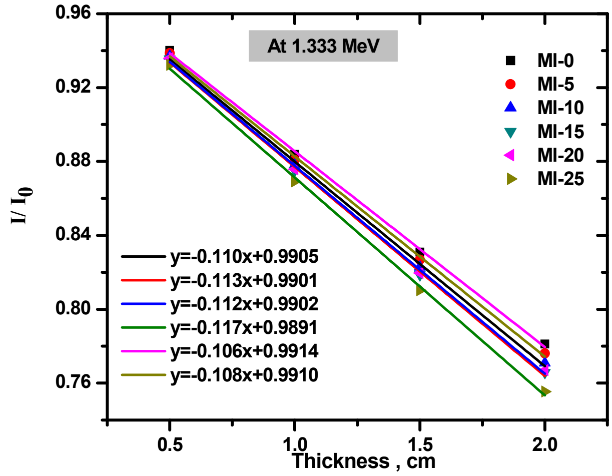

(**d**)

Figure 5. (**a**) The TF of prepared mortar samples at 0.06 MeV with different thicknesses. (**b**) The TF of prepared mortar samples at 0.662 MeV with different thicknesses. (**c**) The TF of prepared mortar samples at 1.173 MeV with different thicknesses. (**d**) The TF of prepared mortar samples at 1.333 MeV with different thicknesses.

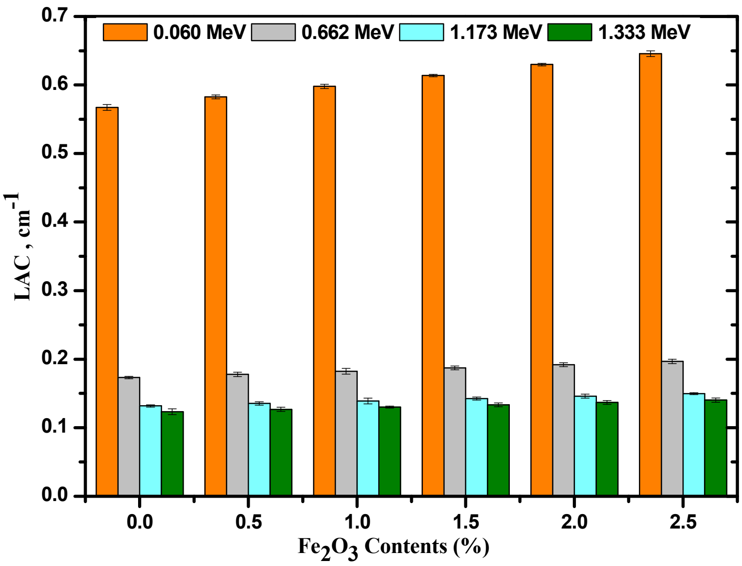

Figure 6. The relation between the LAC and the concentrations of Fe_2O_3 nanoparticles.

The experimental HVL values for the reference mortar and the mortar samples with Fe_2O_3 nanoparticles are given in Figure 7. It was found that the HVL values for the four tested energies decrease as the amount of Fe_2O_3 nanoparticles increases in the mortar. At 0.06 MeV, the HVL for the reference mortar is higher than the other mortar samples (it is 1.223 cm for the reference mortar and varied between 1.19 cm for MI-5 and 1.074 cm for MI-25). At 0.662 MeV, the HVL for the reference mortar is 4.002 cm and decreases to 3.898 cm due to the addition of 5% of Fe_2O_3 nanoparticles, and to 3.524 cm due to the addition of 25% of Fe_2O_3 nanoparticles. So, increasing the ratio of Fe_2O_3 nanoparticles can lead to a notable reduction in the HVL. As we found in the previous figure, the energy of the photons also affects the HVL. It can be seen that the HVL increases significantly due to the increase in the energy from 0.06 to 1.333 MeV. For instance, for MI-5, the HVL varied between 1.190 and 5.468 cm between the lowest and highest investigated energies. So, the HVL at 1.33 MeV is almost 4.5 times the HVL for the same sample (i.e., MI-5) at 0.06 MeV. This result is also valid for the other mortars, where the HVL for MI-15 at 1.333 MeV is almost 4.6 times the HVL of the same mortar at 0.06 MeV.

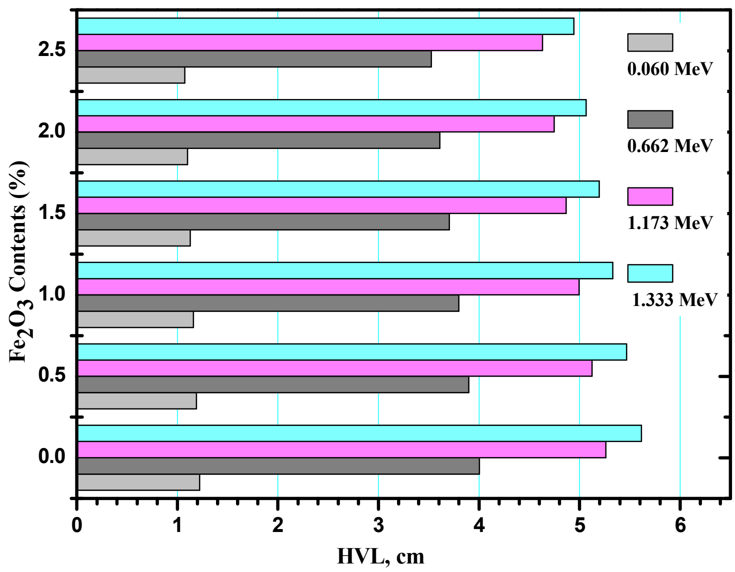

Figure 7. The relation between the HVL and the concentrations of Fe_2O_3 nanoparticles at different energies.

The radiation attenuation competences of the tested mortars have been examined in the context of the tenth value layer (TVL). The experimental results for the TVL have been graphed in Figure 8. According to the data given in this figure, the thinnest TVL and thus the superior radiation shielding competence (3.56, 11.69, 15.36, and 16.40 cm at the selected energies) have been found for the mortar with 25% of Fe_2O_3 nanoparticles. Additionally, the TVL values of the reference mortar were higher than the values predicted for all mortars with 2%–25% of Fe_2O_3 nanoparticles. According to the TVL results, we can develop new mortars for radiation shielding applications by introducing Fe_2O_3 nanoparticles.

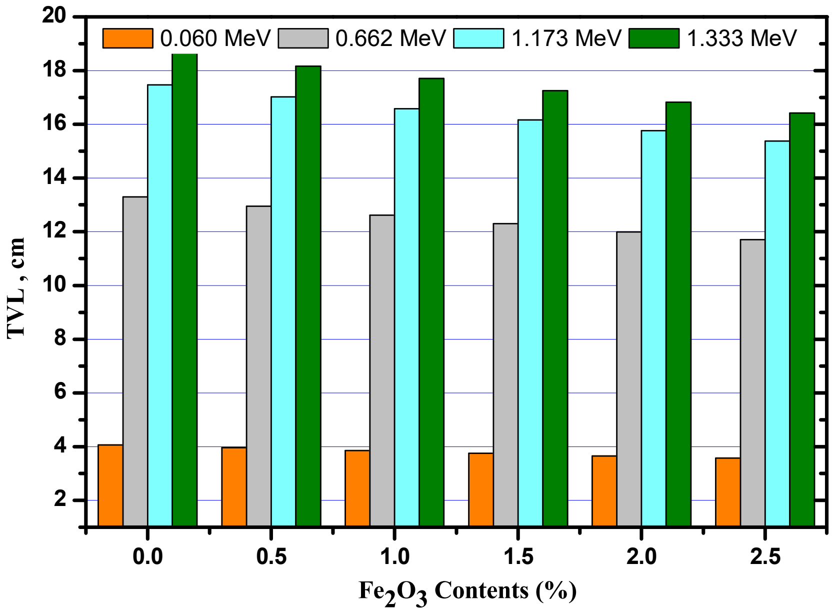

Figure 8. The relation between the TVL and the concentrations of Fe_2O_3 nanoparticles at different energies.

It is also important to examine the radiation absorption ratio (RAR) and to check the impact of the thickness of the mortars on this quantity as shown in Figure 9. So, we selected two thicknesses from each mortar (2 cm and 5 cm) and evaluated the RAR for the mortars with these two thicknesses. If we look at the RAR values for MI-0 at 0.06 MeV, we can see that the RAR is 67.82% for a thickness of 2 cm, but it is 94.13% for MI-0 with a thickness of 5 cm. For MI-10, the RAR at 0.06 MeV is 69.76% for a thickness of 2 cm, and increases to 94.97% for a thickness of 5 cm. At this energy, we noticed that the RAR for MI-0 and MI-10 with a thickness of 5 cm is higher than that of 2 cm, and this is correct for the other mortars. Hence, the thickness of the mortar plays a major role in attenuating the incoming photons. An interesting result is the RAR for MI-25 with a thickness of 5 cm. For this mortar, the RAR at 0.06 MeV is 96.03% which means that this mortar can block almost all the incoming photons with low energy (less than 0.1 MeV). MI-15 and MI-20 with a thickness of 5 cm are also effective mortars in low-energy applications. The results proved that if the space is available, preparing mortar with Fe_2O_3 nanoparticles with a thickness of 5 cm is very useful in radiation shielding applications. When we look at the RAR for both thicknesses at 1.333 MeV, we found that the RAR values reduce to around half, varying between 21.88% (for the reference mortar with a thickness of 2 cm) and 24.46% for MI-25 with the same thickness. Meanwhile, it varied between 46.04 for the reference mortar at 5 cm and 50.40% for MI-25. The mortar at 2 cm has weak attenuation ability for the radiation with energy of 1.333 MeV, while the same mortars with a 5 cm thickness can block about 50% of the radiation with energy higher than 1 MeV.

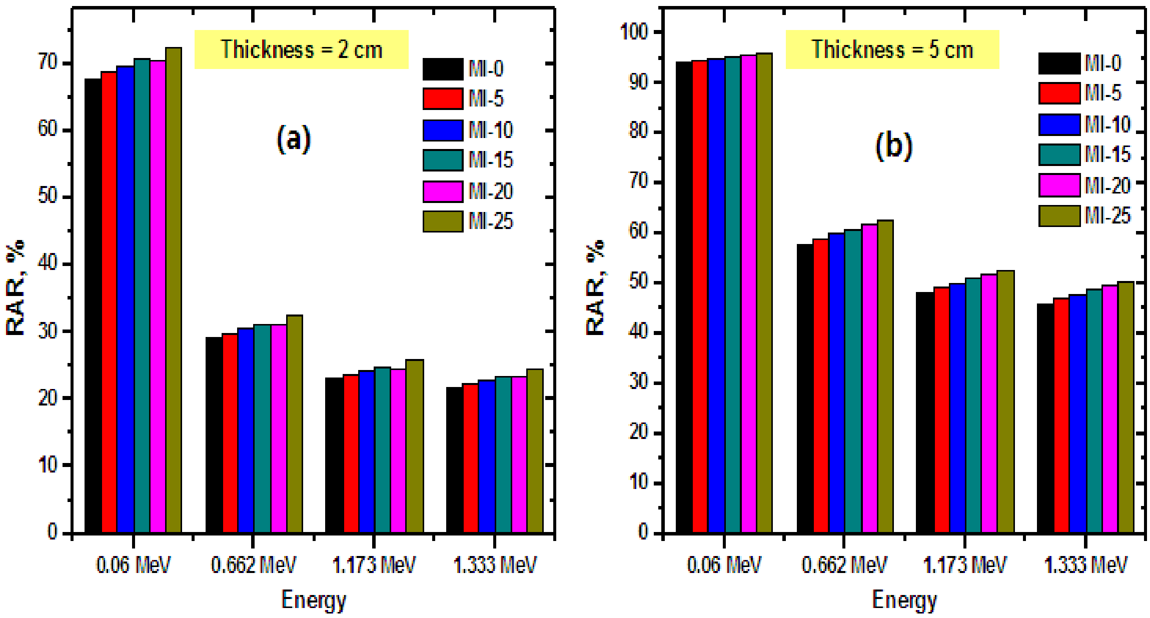

Figure 9. The relation between the RAR and the energy for prepared sample with (**a**) 2 cm and (**b**) 5 cm thickness.

The present prepared mortars were compared with other related literature, including mortar-based ball clay (M1), mortar-based barite (M3) [22], and mortars with ores and minerals additives (MOS30, MOPr30, MOCr30, and MOMg30) [37]. Figure 10 shows the MFP (which equals the reciprocal of LAC and represents the path length without any collisions inside the absorber) of this mortar, and the results indicated that the MI-25 mortar had the lowest MFP compared to the rest of the mortars, for which the MFP was 5.324, 5.135, 5.564, 5.323, 5.279, 5.195, 5.342, 5.209, and 5.084 cm for M1, M3, MOS30, MOPr30, MOCr30, MOMg30, MI-15, M1-20, and MI-25, respectively.

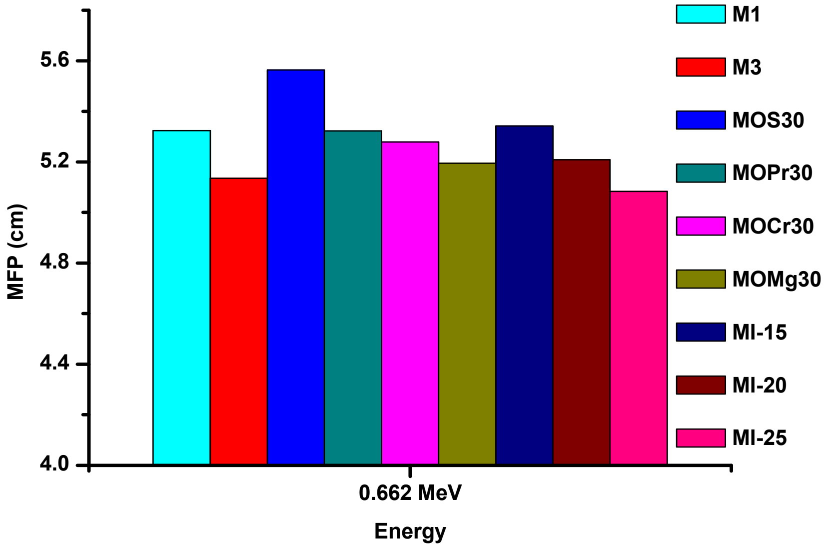

Figure 10. The MFP of prepared samples compared with other related literature.

4. Conclusions

We experimentally reported the attenuation factors for some mortar samples with Fe_2O_3 nanoparticles. We studied the impact of Fe_2O_3 nanoparticles by comparing the reference mortar with the other samples which contain nano-Fe_2O_3. From the relation between the transmission factor (I/I_0) and the thickness of the prepared mortar, we calculated the LAC and, from this parameter, we derived other important factors such as HVL. When we examined the impact of the thickness of the prepared mortars on the attenuation performance of the newly developed samples, we found that increasing the thickness of the mortars led to a decrease in the TF and hence a decrease in the transmission of the photons through the prepared mortars under all the applied energies. Among the different prepared mortars, the lowest TF belongs to the mortar coded as MI-25, which gives an indication about the development in the attenuation ability of the prepared mortar samples due to the addition of Fe_2O_3. When we examined the impact of Fe_2O_3 nanoparticles on the attenuation performance of these samples, we found that the lowest LAC belongs for the reference mortar (free Fe2O_3 nanoparticles). On the contrast, the highest LAC is found for MI-25, which contains the maximum amount of Fe_2O_3. Hence, we can draw a conclusion that increasing the ratio of Fe_2O_3 nanoparticles can lead to a remarkable improvement in the gamma ray shielding. When we examined the impact of the energy of the radiation on the attenuation performance of the newly prepared mortars, we found a high difference in the LAC as well as HVL values between the lowest and highest energies. From the RAR results, we found that MI-25 can block almost all the incoming photons with low energy (less than 0.1 MeV). The RAR results also demonstrated that a mortar of a thickness of 5 cm can be used effectively in radiation shielding applications.

Author Contributions: Conceptualization, M.E. and M.I.S.; methodology, M.E.; software, N.A.; validation, M.I.S., M.E. and N.A.; formal analysis, N.A.; investigation, M.E.; resources, N.A.; data curation, M.I.S.; writing—original draft preparation, M.E.; writing—review and editing, M.I.S.; visualization, N.A.; supervision, M.E.; project administration, M.I.S.; funding acquisition, N.A. All authors have read and agreed to the published version of the manuscript.

Funding: The authors express their gratitude to Princess Nourah bint Abdulrahman University Researchers Supporting Project Number (PNURSP2022R111), Princess Nourah bint Abdulrahman University, Riyadh, Saudi Arabia.

Institutional Review Board Statement: Not applicable.

Informed Consent Statement: Not applicable.

Data Availability Statement: Not applicable.

Acknowledgments: The authors express their gratitude to Princess Nourah bint Abdulrahman University Researchers Supporting Project Number (PNURSP2022R111), Princess Nourah bint Abdulrahman University, Riyadh, Saudi Arabia.

Conflicts of Interest: The authors declare no conflict of interest.

References

1. Aygün, B. Neutron and gamma radiation shielding Ni based new type super alloys development and production by Monte Carlo Simulation technique. *Radiat. Phys. Chem.* **2021**, *188*, 109630. [CrossRef]
2. Kamislioglu, M. An investigation into gamma radiation shielding parameters of the (Al:Si) and (Al + Na):Si-doped international simple glasses (ISG) used in nuclear waste management, deploying Phy-X/PSD and SRIM software. *J. Mater. Sci. Mater. Electron.* **2021**, *32*, 12690–12704. [CrossRef]
3. Abouhaswa, A.S.; Kavaz, E. Bi_2O_3 effect on physical, optical, structural and radiation safety characteristics of B_2O_3-Na_2O-ZnO-CaO glass system. *J. Non Cryst. Solids* **2020**, *535*, 119993. [CrossRef]
4. Dong, M.; Xue, X.; Yang, H.; Li, Z. Highly cost-effective shielding composite made from vanadium slag and boron-rich slag and its properties. *Radiat. Phys. Chem.* **2017**, *141*, 239–244. [CrossRef]
5. Dong, M.; Xue, X.; Yang, H.; Liu, D.; Wang, C.; Li, Z. A novel comprehensive utilization of vanadium slag: As gamma ray shielding material. *J. Hazard. Mater.* **2016**, *318*, 751–757. [CrossRef] [PubMed]
6. Dong, M.; Zhou, S.; Xue, X.; Sayyed, M.; Tishkevich, D.; Trukhanov, A.; Wang, C. Study of comprehensive shielding behaviors of chambersite deposit for neutron and gamma ray. *Prog. Nucl. Energy* **2022**, *146*, 104155. [CrossRef]
7. Aygün, B. High alloyed new stainless steel shielding material for gamma and fast neutron radiation. *Nucl. Eng. Technol.* **2019**, *52*, 647–653. [CrossRef]
8. Rajesh, M.; Kavaz, E.; Deva, B.; Raju, P. Photoluminescence, radiative shielding properties of Sm^{3+} ions doped fluoroborosilicate glasses for visible (reddish-orange) display and radiation shielding applications. *Mater. Res. Bull.* **2021**, *142*, 111383. [CrossRef]

9. Al-Yousef, H.A.; Alotiby, M.; Hanfi, M.Y.; Alotaibi, B.M.; Mahmoud, K.A.; Sayyed, M.I.; Al-Hadeethi, Y. Effect of the Fe_2O_3 addition on the elastic and gamma-ray shielding features of bismuth sodium-borate glass system. *J. Mater. Sci. Mater. Electron.* **2021**, *32*, 6942–6954. [CrossRef]
10. Albarzan, B.; Hanfi, M.Y.; Almuqrin, A.H.; Sayyed, M.I.; Alsafi, H.M.; Mahmoud, K.A. The Influence of Titanium Dioxide on Silicate-Based Glasses: An Evaluation of the Mechanical and Radiation Shielding Properties. *Materials* **2021**, *14*, 3414. [CrossRef]
11. Naseer, K.; Sathiyapriya, G.; Marimuthu, K.; Piotrowski, T.; Alqahtani, M.S.; Yousef, E.S. Optical, elastic, and neutron shielding studies of Nb_2O_5 varied Dy^{3+} doped barium-borate glasses. *Optik* **2021**, *251*, 168436. [CrossRef]
12. Zayed, A.M.; Masoud, M.A.; Shahien, M.G.; Gökçe, H.S.; Sakr, K.; Kansouh, W.A.; El-Khayatt, A.M. Physical, mechanical and radiation attenuation properties of serpentine concrete containing boric acid. *Constr. Build. Mater.* **2021**, *272*, 121641. [CrossRef]
13. Gökçe, H.S.; Öztürk, B.C.; Çam, N.F.; Andiç-Çakır, Ö. Gamma-ray attenuation coefficients and transmission thickness of high consistency heavyweight concrete containing mineral admixture. *Cem. Concr. Compos.* **2018**, *92*, 56–69. [CrossRef]
14. Abbas, M.I.; El-Khatib, A.M.; Dib, M.F.; Mustafa, H.E.; Sayyed, M.I.; Elsafi, M. The Influence of Bi_2O_3 Nanoparticle Content on the γ-ray Interaction Parameters of Silicon Rubber. *Polymers* **2022**, *14*, 1048. [CrossRef]
15. Nikbin, I.M.; Rafiee, A.; Dezhampanah, S.; Mehdipour, S.; Mohebbi, R.; Moghadam, H.H.; Sadrmomtazi, A. Effect of high temperature on the radiation shielding properties of cementitious composites containing nano-Bi_2O. *J. Mater. Res. Technol.* **2020**, *9*, 11135–11153. [CrossRef]
16. Nikbin, I.M.; Mohebbi, R.; Dezhampanah, S.; Mehdipour, S.; Mohammadi, R.; Nejat, T. Gamma ray shielding properties of heavy-weight concrete containing Nano-TiO. *Radiat. Phys. Chem.* **2019**, *162*, 157–167. [CrossRef]
17. El-Sayed, T.A. Performance of heavy weight concrete incorporating recycled rice straw ash as radiation shielding material. *Prog. Nucl. Energy* **2021**, *135*, 103693. [CrossRef]
18. El-Sayed, A.A.; Fathy, I.N.; Tayeh, B.A.; Almeshal, I. Using artificial neural networks for predicting mechanical and radiation shielding properties of different nano-concretes exposed to elevated temperature. *Constr. Build. Mater.* **2022**, *324*, 126663. [CrossRef]
19. Abo-El-Enein, S.; El-Hosiny, F.; El-Gamal, S.; Amin, M.; Ramadan, M. Gamma radiation shielding, fire resistance and physicochemical characteristics of Portland cement pastes modified with synthesized Fe_2O_3 and ZnO nanoparticles. *Constr. Build. Mater.* **2018**, *173*, 687–706. [CrossRef]
20. Seifan, M.; Mendoza, S.; Berenjian, A. Mechanical properties and durability performance of fly ash based mortar containing nano- and micro-silica additives. *Constr. Build. Mater.* **2020**, *252*, 119121. [CrossRef]
21. Glinicki, M.A.; Antolik, A.; Gawlicki, M. Evaluation of compatibility of neutron-shielding boron aggregates with Portland cement in mortar. *Constr. Build. Mater.* **2018**, *164*, 731–738. [CrossRef]
22. Sayyed, M.I.; Elsafi, M.; Almuqrin, A.H.; Cornish, K.; Elkhatib, A.M. Novel Shielding Mortars for Radiation Source Transportation and Storage. *Sustainability* **2022**, *14*, 1248. [CrossRef]
23. Sayyed, M.; Hamad, M.K.; Mhareb, M.; Kurtulus, R.; Dwaikat, N.; Saleh, M.; Elsafi, M.; Taki, M.M.; Kavas, T.; Ziq, K.; et al. Assessment of radiation attenuation properties for novel alloys: An experimental approach. *Radiat. Phys. Chem.* **2022**, 110152. [CrossRef]
24. Şensoy, A.T.; Gökçe, H.S. Simulation and optimization of gamma-ray linear attenuation coefficients of barite concrete shields. *Constr. Build. Mater.* **2020**, *253*, 119218. [CrossRef]
25. Demir, I.; Gümüş, M.; Gökçe, H.S. Gamma ray and neutron shielding characteristics of polypropylene fiber-reinforced heavyweight concrete exposed to elevated temperatures. *Constr. Build. Mater.* **2020**, *257*, 119596. [CrossRef]
26. Kaewjaeng, S.; Kothan, S.; Chaiphaksa, W.; Chanthima, N.; Rajaramakrishna, R.; Kim, H.J.; Kaewkhao, J. High transparency La_2O_3-CaO-B_2O_3-SiO_2 glass for diagnosis x-rays shielding material application. *Radiat. Phys. Chem.* **2019**, *160*, 41–47. [CrossRef]
27. D'Souza, A.N.; Sayyed, M.; Karunakara, N.; Al-Ghamdi, H.; Almuqrin, A.H.; Elsafi, M.; Khandaker, M.U.; Kamath, S.D. TeO_2–SiO_2–B_2O_3 glasses doped with CeO_2 for gamma radiation shielding and dosimetry application. *Radiat. Phys. Chem.* **2022**, 110233. [CrossRef]
28. Kaewjaeng, S.; Chanthima, N.; Thongdang, J.; Reungsri, S.; Kothan, S.; Kaewkhao, J. Synthesis and radiation properties of Li_2O-BaO-Bi_2O_3-P_2O_5 glasses. *Mater. Today Proc.* **2021**, *43*, 2544–2553. [CrossRef]
29. Chanthima, N.; Kaewkhao, J.; Limkitjaroenporn, P.; Tuscharoen, S.; Kothan, S.; Tungjai, M.; Kaewjaeng, S.; Sarachai, S.; Limsuwan, P. Development of BaO–ZnO–B_2O_3 glasses as a radiation shielding material. *Radiat. Phys. Chem.* **2017**, *137*, 72–77. [CrossRef]
30. Tijani, S.A.; Al-Hadeethi, Y.F. The use of isophthalic-bismuth polymer composites as radiation shielding barriers in nuclear medicine. *Mater. Res. Express* **2019**, *6*, 055323. [CrossRef]
31. Cheewasukhanont, W.; Limkitjaroenporn, P.; Kothan, S.; Kedkaew, C.; Kaewkhao, J. The effect of particle size on radiation shielding properties for bismuth borosilicate glass. *Radiat. Phys. Chem.* **2020**, *172*, 108791. [CrossRef]
32. Hannachi, E.; Sayyed, M.I.; Slimani, Y.; Almessiere, M.A.; Baykal, A.; Elsafi, M. Synthesis, characterization, and performance assessment of new composite ceramics towards radiation shielding applications. *J. Alloys Compd.* **2022**, *899*, 163173. [CrossRef]
33. Elsafi, M.; Koraim, Y.; Almurayshid, M.; Almasoud, F.I.; Sayyed, M.I.; Saleh, I.H. Investigation of Photon Radiation Attenuation Capability of Different Clay Materials. *Materials* **2021**, *14*, 6702. [CrossRef]
34. Elsafi, M.; Dib, M.F.; Mustafa, H.E.; Sayyed, M.I.; Khandaker, M.U.; Alsubaie, A.; Almalki, A.S.A.; Abbas, M.I.; El-Khatib, A.M. Enhancement of Ceramics Based Red-Clay by Bulk and Nano Metal Oxides for Photon Shielding Features. *Materials* **2021**, *14*, 7878. [CrossRef]

35. Elsafi, M.; El-Nahal, M.A.; Alrashedi, M.F.; Olarinoye, O.I.; Sayyed, M.I.; Khandaker, M.U.; Osman, H.; Alamri, S.; Abbas, M.I. Shielding Properties of Some Marble Types: A Comprehensive Study of Experimental and XCOM Results. *Materials* **2021**, *14*, 4194. [CrossRef]
36. Agar, O.; Sayyed, M.I.; Tekin, H.O.; Kaky, K.M.; Baki, S.O.; Kityk, I. An investigation on shielding properties of BaO, MoO_3 and P_2O_5 based glasses using MCNPX code. *Results Phys.* **2019**, *12*, 629–634. [CrossRef]
37. Baltas, H.; Sirin, M.; Celik, A.; Ustabas, İ.; El-Khayatt, A.M. Radiation shielding properties of mortars with minerals and ores additives. *Cem. Concr. Compos.* **2019**, *97*, 268–278. [CrossRef]